By considering separately each type of power-law noise, evaluation of the integral relationships provided in Equation (5.113) for the true variance, in Equation (5.114) for the M-sample variance, in Equation (5.115) for the Allan variance, in Equation (5.117) for the modified Allan variance, in Equation (5.120) for the Time variance and in Equation (5.121) for the $\mathrm{TIE}_{\mathrm{rms}}$ yields the corresponding time-domain expressions.

It is worthwhile noticing, at this point, that evaluation of those integrals features two critical points: for $f \to 0$ and for $f \to \infty$. Convergence for $f \to \infty$ is ensured by the upper cut-off frequency f_{h} in the model defined in Equation (5.125). Convergence for $f \to 0$, on the other hand, gets tougher as higher is the exponent of the Fourier frequency f at the denominator of Equation (5.125). For example, we noted that $I^2(\tau) \to \infty$ if $S_y(f) \propto f^{-1}$. The asymptotic behaviour for $f \to 0$ of the transfer function associated to other stability quantities ensures convergence even for $S_y(f) \propto f^{-4}$.

The results are summarized in the synoptical Tables 5.2 through 5.7, reporting for each power-law noise type the corresponding expressions of the true variance $I^2(\tau)$, of the M-sample variance $\langle \sigma_y^2(M, \tau, \tau) \rangle$, of the Allan variance $\sigma_y^2(\tau)$, of the modified Allan variance $\mathrm{mod}\sigma_y^2(\tau)$, of the Time variance $\sigma_x^2(\tau)$ and of the root mean square of the Time Interval Error $\mathrm{TIE}_{\mathrm{rms}}(\tau)$.

An important remark is that including an upper cut-off frequency f_{h} in the model (5.125) is necessary, in order to ensure convergence of integrals for $f \to \infty$ also for WPM and FPM noise types. This upper cut-off frequency should always be specified, when due to the measurement instrumentation and not modelling the actual behaviour of the clock under test, because WPM and FPM noise measurement results depend on its value, as evident from Tables 5.2 through 5.7. In other words, measurements accomplished with test set-ups having different bandwidths may yield to different results. Moreover, results reported in tables above are valid only for $\tau \gg 1/(2\pi f_{\mathrm{h}})$, which is the most common case in practical measurements.

5.10.1.1 *Expressions of the True Variance and of the M-Sample Variance*

The expressions for the true variance reported in Table 5.2 can be derived by those for the M-sample variance in Table 5.3 by letting $T = \tau$ and evaluating the limit $M \to \infty$. Moreover, by inspection of the same tables, it is evident that these two variances depend, for FFM and RWFM noise, on the number M of samples and tend to infinite for $M \to \infty$.

Table 5.2 Expressions of the true variance for each power-law noise type

Noise Type	$S_x(f)$	$I^2(\tau)$
WPM	h_2	$\frac{1}{4\pi^2} h_2 f_{\mathrm{h}} \cdot \tau^{-2}$ for $\tau \gg 1/(2\pi f_{\mathrm{h}})$
FPM	h_1/f	$\frac{h_1}{2\pi^2}[\gamma + \log(2\pi f_h \tau)] \cdot \tau^{-2}$ for $\tau \gg 1/(2\pi f_{\mathrm{h}})$
WFM	h_0/f^2	$\frac{h_0}{2} \cdot \tau^{-1}$
FFM	h_{-1}/f^3	$\lim_{M\to\infty} \frac{M \log M}{M-1} h_{-1} = \infty$
RWFM	h_{-2}/f^4	$\lim_{M\to\infty} \frac{\pi^2}{3} M h_{-2} \cdot \tau = \infty$

$\gamma = 0.5772156649\ldots$ (Euler's constant)

Table 5.3 Expressions of the M-sample variance for each power-law noise

Noise Type	$S_x(f)$	$\langle \sigma_y^2(M, \tau, \tau) \rangle$
WPM	h_2	$2\frac{M + \delta_K(r-1)}{M4\pi^2} h_2 f_{\mathrm{h}} \cdot \tau^{-2}$ for $\tau \gg 1/(2\pi f_{\mathrm{h}})$
FPM	h_1/f	$\left\{\gamma + \log(2\pi f_{\mathrm{h}}\tau) + \frac{1}{M(M-1)} \sum_{n=1}^{M-1} (M-n) \log\left[\frac{n^2 r^2}{n^2 r^2 - 1}\right]\right\} \cdot \frac{h_1}{2\pi^2} \cdot \tau^{-2}$ for $r \gg 1$ and $\tau \gg 1/(2\pi f_{\mathrm{h}})$
WFM	h_0/f^2	$\frac{h_0}{2} \cdot \tau^{-1}$ for $r \gg 1$
FFM	h_{-1}/f^3	$\left\{\sum_{n=1}^{M} (M-n)\left[-2(nr)^2 \log(nr) + (nr+1)^2 \log(nr+1) + (nr-1)^2 \log|nr-1|\right]\right\} \cdot \frac{h_{-1}}{M(M-1)}$
RWFM	h_{-2}/f^4	$\frac{\pi^2}{3}[r(M+1) - 1] h_{-2} \cdot \tau$ for $r \geq 1$

$r = \frac{T}{\tau}$, $\delta_K(n) = \begin{cases} 1 & \text{for } n = 0 \\ 0 & \text{for } n \neq 0 \end{cases}$, $\gamma = 0.5772156649\ldots$ (Euler's constant)

Table 5.4 Expressions of the Allan variance for each power-law noise type

Noise Type	$S_x(f)$	$\sigma_y^2(\tau)$
WPM	h_2	$\frac{3}{4\pi^2} h_2 f_{\mathrm{h}} \cdot \tau^{-2}$ for $\tau \gg 1/(2\pi f_{\mathrm{h}})$
FPM	h_1/f	$\frac{h_1}{4\pi^2}\{3[\gamma + \log(2\pi f_{\mathrm{h}}\tau)] - \log 2\} \cdot \tau^{-2}$ for $\tau \gg 1/(2\pi f_{\mathrm{h}})$
WFM	h_0/f^2	$\frac{h_0}{2} \cdot \tau^{-1}$
FFM	h_{-1}/f^3	$2\log 2 \cdot h_{-1}$
RWFM	h_{-2}/f^4	$\frac{2\pi^2}{3} h_{-2} \cdot \tau$

$\gamma = 0.5772156649\ldots$ (Euler's constant)

Hence, true variance and M-sample variance are not suitable for clock stability characterization in presence of these types of noise.

5.10.1.2 *Expressions of the Allan Variance*

As far as the Allan variance is concerned, from Table 5.4 it is important to notice the following features.

- The Allan variance quantity is convergent for all kinds of power-law noise. Its convergence to a finite value for $f \to 0$, even for FFM and RWFM noise, is ensured by the asymptotic behaviour of the transfer function $H_{\mathrm{A}}(f)$, in integral (5.115), which behaves as $\sim f^2$ for $f \to 0$.

- For all the five types of frequency-domain power-law noise ($\alpha = 0, -1, -2, -3, -4$), the Allan variance obeys in turn to a time-domain power law of the form

$$\sigma_y^2(\tau) = A_\mu \tau^\mu \tag{5.126}$$

(for $\mu = -2, -1, 0, +1$) with a slight modification for FPM noise because of the logarithm[17]. Therefore, a log–log plot of $\sigma_y^2(\tau)$ exhibits segments of straight lines, one per each noise type, whose slopes may be easily identified, as shown in the example diagram of Figure 5.29 (cf. Figure 5.23).

- Allan variance measurement results can thus be interpreted to identify the different types of power-law noise. Nevertheless, since both WPM and FPM noises yield very similar slopes, there is some ambiguity in noise identification whenever $\sigma_y^2(\tau) \propto \tau^{-2}$ is measured

5.10.1.3 *Expressions of the Modified Allan Variance*

As far as the modified Allan variance is concerned, on the other hand, the analytical evaluation of integral (5.117) proves quite cumbersome. As already mentioned, several works discussed in detail the properties of this quantity [5.24][5.26][5.28][5.29]. In particular, it has been studied the behaviour of the ratio

$$R(n) = \frac{\mathrm{mod}\sigma_y^2(\tau)}{\sigma_y^2(\tau)} \tag{5.127}$$

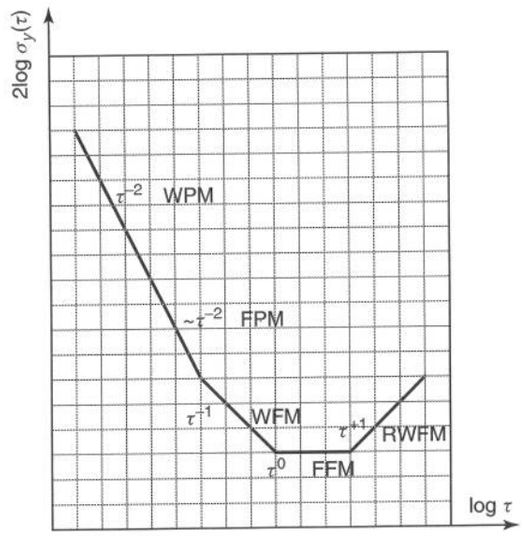

Figure 5.29. Sample log–log plot of the Allan variance in presence of power-law noise

[17] Also the true variance and the M-sample variance exhibit a similar behaviour, but the fact that they do not converge for some types of power-law noise makes their time-domain power law less remarkable.

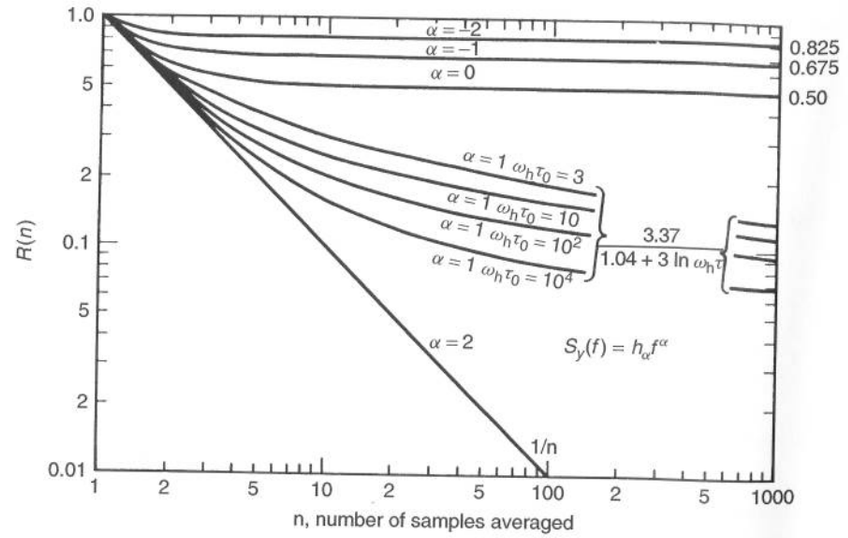

Figure 5.30. Ratio $R(n)$ for all types of power-law noise. (Reproduced from [5.29], NIST. Not copyrightable)

where, once again, $n = \tau/\tau_0$. This ratio is plotted in Figure 5.30 (from [5.29], Section A6) versus n, for all types of power-law noise[18] and also for different values of the product $2\pi f_h \tau_0$, when relevant. The graph in Figure 5.30 was obtained directly from the basic definitions of the plain and modified Allan variances, by numerical computation. By inspection of this graph, we notice that:

- for WPM noise, the ratio $R(n)$ is $1/n$; therefore, for any given sampling period τ_0, while $\sigma_y^2(\tau)$ behaves as τ^{-2}, mod $\sigma_y^2(\tau)$ behaves as τ^{-3};
- for WFM, FFM and RWFM noises, the ratio $R(n)$ reaches quickly an asymptotic value for $n > 10$ (cf. Figure 5.20);
- for FPM noise, the value of the ratio $R(n)$ depends on the upper cut-off frequency f_h of the noise processes measured (as already pointed out, this cut-off frequency is the lower between the measurement hardware bandwidth and the clock hardware bandwidth); moreover, in this case, an asymptotic value is approached for at least $n > 100$.

In conclusion, from the results plotted in the diagram of Figure 5.30, from Equation (5.127) and from the expressions in Table 5.4, it is possible to derive the asymptotic expressions (i.e., strictly valid for $n \to \infty$ and keeping $n\tau_0 = \tau$ constant) reported in Table 5.5.

By inspection of these expressions, therefore, we notice that also the modified Allan variance, for all the five types of frequency-domain power-law noise, obeys in turn to

[18] Note that, in Figure 5.30, α denotes the exponent of the Fourier frequency in the PSD $S_y(f)$ rather than in $S_x(f)$ as we used elsewhere in this chapter. Hence, power-law noise types here are indexed by values of α from $\alpha = -2$ (RWFM) to $\alpha = 2$ (WPM).

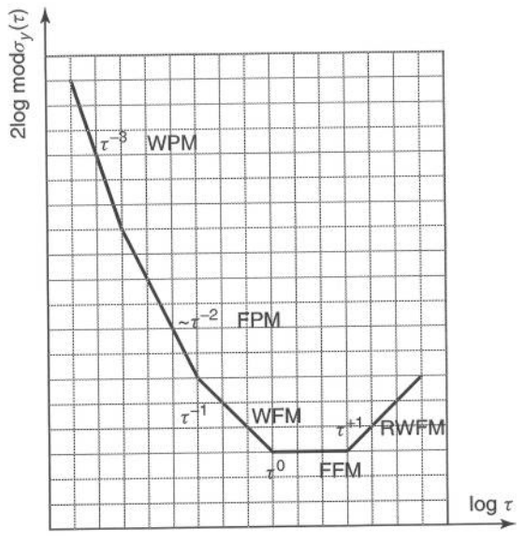

Figure 5.31. Sample log–log plot of the modified Allan variance in presence of power-law noise

a time-domain power law of the form (5.126), as shown in the example diagram of Figure 5.31 (cf. Figure 5.29). Thus, modified Allan variance measurement results can be interpreted to identify the different types of power-law noise, but without the ambiguity between WPM and FPM noises as with Allan variance.

5.10.1.4 Expressions of the Time Variance

It is straightforward to extend all considerations about the modified Allan variance to the Time variance, based on its definition (5.94), and thus to derive the expressions reported in Table 5.6 from those in Table 5.5.

Moreover, as obvious, the Time variance obeys the same time-domain power law as the modified Allan variance (cf. Figure 5.31), having added +2 to the exponent μ.

5.10.1.5 Expressions of the Root Mean Square of the Time Interval Error

From the relationship between the root mean square of the Time Interval Error and the true variance in Equation (5.97), it is straightforward to derive the expressions reported in Table 5.7 from those in Table 5.2.

5.10.1.6 Summary of Relationships between Frequency-Domain and Time-Domain Power Laws

To reader's ease, in Table 5.8 we summarize the various values of the exponent μ (i.e., the slopes in log–log plots) in time-domain power laws such as Equation (5.126), for the stability quantities considered and for all types of power-law noise, resulting from expressions reported in Tables 5.2 through 5.7. In other words, for each type of power-law noise, having spectrum $S_x(f) = h_{\alpha+2}/f^{\alpha}$, it is specified the power τ^{μ} to which the stability quantity considered is proportional.

Table 5.5 Asymptotic expressions of the modified Allan variance for each power-law noise (strictly valid for $n \to \infty$ and keeping $n\tau_0 = \tau$ constant)

Noise Type	$S_x(f)$	$\mathrm{mod}\sigma_y^2(\tau)$
WPM	h_2	$\frac{1}{n} \cdot \frac{3}{4\pi^2} h_2 f_h \cdot \tau^{-2}$ for $\tau \gg 1/(2\pi f_h)$
FPM	h_1/f	$\frac{3.37}{1.04 + 3\log(2\pi f_h \tau)} \cdot \frac{h_1}{4\pi^2} \{3[\gamma + \log(2\pi f_h \tau)] - \log 2\} \cdot \tau^{-2}$ for $\tau \gg 1/(2\pi f_h)$ and $n > 100$
WFM	h_0/f^2	$\frac{1}{2} \cdot \frac{h_0}{2} \cdot \tau^{-1}$ for $n > 10$
FFM	h_{-1}/f^3	$0.675 \cdot 2\log 2 \cdot h_{-1}$ for $n > 10$
RWFM	h_{-2}/f^4	$0.825 \cdot \frac{2\pi^2}{3} h_{-2} \cdot \tau$ for $n > 10$

$\tau = n\tau_0$, $\gamma = 0.5772156649\ldots$ (Euler's constant)

Table 5.6 Asymptotic expressions of the Time variance for each power-law noise (strictly valid for $n \to \infty$ and keeping $n\tau_0 = \tau$ constant)

Noise Type	$S_x(f)$	$\sigma_x^2(\tau)$
WPM	h_2	$\frac{1}{n} \cdot \frac{h_2 f_h}{4\pi^2}$ for $\tau \gg 1/(2\pi f_h)$
FPM	h_1/f	$\frac{3.37}{1.04 + 3\log(2\pi f_h \tau)} \cdot \frac{h_1}{12\pi^2} \{3[\gamma + \log(2\pi f_h \tau)] - \log 2\}$ for $\tau \gg 1/(2\pi f_h)$ and $n > 100$
WFM	h_0/f^2	$\frac{h_0}{12} \cdot \tau$ for $n > 10$
FFM	h_{-1}/f^3	$\frac{0.675 \cdot 2\log 2}{3} h_{-1} \cdot \tau^2$ for $n > 10$
RWFM	h_{-2}/f^4	$\frac{0.825 \cdot 2\pi^2}{9} h_{-2} \cdot \tau^3$ for $n > 10$

$\tau = n\tau_0$, $\gamma = 0.5772156649\ldots$ (Euler's constant)

Table 5.7 Expressions of the root mean square of the Time Interval Error for each power-law noise type

Noise Type	$S_x(f)$	$\mathrm{TIE}_{\mathrm{rms}}(\tau)$
WPM	h_2	$\sqrt{\frac{1}{4\pi^2} h_2 f_h}$ for $\tau \gg 1/(2\pi f_h)$
FPM	h_1/f	$\sqrt{\frac{h_1}{2\pi^2}[\gamma + \log(2\pi f_h \tau)]}$ for $\tau \gg 1/(2\pi f_h)$
WFM	h_0/f^2	$\sqrt{\frac{h_0}{2}\tau}$
FFM	h_{-1}/f^3	not convergent
RWFM	h_{-2}/f^4	not convergent

$\gamma = 0.5772156649\ldots$ (Euler's constant)

Table 5.8 Relationships between frequency-domain and time-domain power laws for stability quantities measured on autonomous clocks

Noise Type	$S_x(f)$	$I^2(\tau)$	$\langle\sigma_y^2(M,\tau,\tau)\rangle$	$\sigma_y^2(\tau)$	mod $\sigma_y^2(\tau)$	$\sigma_x^2(\tau)$	$\mathrm{TIE}_{\mathrm{rms}}(\tau)$
WPM	h_2	τ^{-2}	τ^{-2}	τ^{-2}	τ^{-3}	τ^{-1}	τ^{0}
FPM	h_1/f	τ^{-2}	τ^{-2}	τ^{-2}	τ^{-2}	τ^{0}	τ^{0}
WFM	h_0/f^2	τ^{-1}	τ^{-1}	τ^{-1}	τ^{-1}	τ^{+1}	$\tau^{+1/2}$
FFM	h_{-1}/f^3	—	—	τ^{0}	τ^{0}	τ^{+2}	—
RWFM	h_{-2}/f^4	—	—	τ^{+1}	τ^{+1}	τ^{+3}	—

— = Not convergent

5.10.2 Frequency Offset and Drift

As stated previously in Section 5.8.9, according to international standards, plain TE(t) samples are used to evaluate not only TIErms and MTIE, but also ADEV, MADEV and TDEV, which have been theoretically defined in terms of the $x(t)$ process (5.11). This fact well justifies the need of investigating the effects of frequency offset and drift on the behaviour of the various stability quantities.

If we assume that the reference clock is supplying the ideal time and that a constant frequency offset $\Delta\nu$ and a linear frequency drift D are the only non-ideal components in the timing signal under test, then, considering Equations (5.9), (5.10), (5.12) and (5.13), we have

$$\mathrm{TE}(t) = \frac{\Delta\nu}{\nu_{\mathrm{n}}}t + \frac{D}{2}t^2 \tag{5.128}$$

Now, substituting the TE(t) (5.128) in place of $x(t)$ within the definition of Allan variance (5.91), we get

$$\sigma_y^2(\tau) = \frac{1}{2\tau^2}\left\langle\left[D\tau^2\right]^2\right\rangle = \frac{D^2}{2}\tau^2 \tag{5.129}$$

Therefore, the Allan variance is independent on a constant frequency offset $\Delta\nu$, but it reveals a linear frequency drift D according to a quadratic dependence on the observation interval τ. Note that no power-law noise yields a similar dependence of the Allan variance on τ.

On an analogous fashion, substituting the TE(t) (5.128) in place of $x(t)$ within the definition of modified Allan variance (5.93), we get

$$\begin{aligned}\mathrm{mod}\sigma_y^2(\tau) &= \frac{1}{2\tau^2}\left\langle\left[\frac{1}{n}\sum_{j=1}^{n}(\mathrm{TE}_{j+2n} - 2\mathrm{TE}_{j+n} + \mathrm{TE}_j)\right]^2\right\rangle \\ &= \frac{1}{2\tau^2}\left\langle\left[\frac{1}{n}\sum_{j=1}^{n}D\tau^2\right]^2\right\rangle = \frac{D^2}{2}\tau^2\end{aligned} \tag{5.130}$$

Therefore, the same considerations made for the Allan variance hold also for the modified Allan variance.

Table 5.9 Time-domain power laws for stability quantities in presence of constant frequency offset and linear frequency drift in the underlying TE data

Frequency Impairment	$\sigma_y^2(\tau)$	mod$\sigma_y^2(\tau)$	$\sigma_x^2(\tau)$	$\mathrm{TIE}_{\mathrm{rms}}(\tau)$
constant offset $\nu(t) = \nu_{\mathrm{n}} + \Delta\nu$	not revealed	not revealed	not revealed	τ^{+1}
linear drift $\nu(t) = \nu_{\mathrm{n}} + D\nu_{\mathrm{n}}t$	τ^{+2}	τ^{+2}	τ^{+4}	—

— = Not convergent

From the definition (5.94), we immediately get the expression of the Time variance in presence of a constant frequency offset $\Delta\nu$ and a linear frequency drift D, as

$$\sigma_x^2(\tau) = \frac{D^2}{6}\tau^4 \tag{5.131}$$

As far as the root mean square of the Time Interval Error is concerned, substituting the TE(t) (5.128) in place of $x(t)$ within the definition (5.95), we get

$$\mathrm{TIE}_{\mathrm{rms}}(t;\tau) = \sqrt{E\left\{\left[\frac{\Delta\nu}{\nu_n}\tau + Dt\tau + \frac{D^2}{2}\tau^2\right]^2\right\}} \tag{5.132}$$

Therefore, the root mean square of the Time Interval Error is dependent both on the frequency offset $\Delta\nu$ and on the frequency drift D. What's more, in presence of a frequency drift, it is even not a stationary quantity, being dependent not only on the observation interval τ, but also on the actual measurement time t.

Finally, to reader's ease, we complete previous Table 5.8 by summarizing in Table 5.9 the further results presented in this section.

5.10.3 Periodic Noise

Let us assume that the timing signal under measurement, with nominal frequency ν_{n}, is frequency modulated by a sinusoidal signal of peak amplitude $\Delta\nu_{\mathrm{n}}$ and frequency f_{m}, i.e.

$$y(t) = \frac{\Delta\nu_{\mathrm{n}}}{\nu_{\mathrm{n}}}\sin 2\pi f_{\mathrm{m}}t \tag{5.133}$$

Then, in the frequency domain, the PSD will exhibit a discrete line at the modulation frequency f_{m}, as

$$S_y(t) = \frac{1}{2}\left(\frac{\Delta\nu_{\mathrm{n}}}{\nu_{\mathrm{n}}}\right)^2\delta(f - f_{\mathrm{m}}) \tag{5.134}$$

In the time domain, considering for example the Allan variance, substitution of Equation (5.134) in Equation (5.115) yields

$$\sigma_y^2(\tau) = \left(\frac{\Delta\nu_{\mathrm{n}}}{\nu_{\mathrm{n}}}\right)^2\frac{\sin^4\pi\tau f_{\mathrm{m}}}{(\pi\tau f_{\mathrm{m}})^2} \tag{5.135}$$

Therefore, the effect of a sinusoidal frequency modulation is null whenever τ equals the modulation period $T_m = 1/f_m$ or one of its integer multiples, since the modulating signal is completely averaged out. The maximum effect, on the other hand, occurs when τ is near $T_m/2$ or one of its integer multiples.

Similar results can be obtained for other time-domain stability quantities. For example, for the modified Allan variance, we get

$$\mathrm{mod}\sigma_y^2(\tau) = \left(\frac{\Delta\nu_n}{\nu_n}\right)^2 \left[2\frac{\sin^3 n\tau_0 f_m}{n\tau_0 f_m \sin \tau_0 f_m}\right]^2 \tag{5.136}$$

Seen from another point of view, this effect is, neither more nor less, the *aliasing* of the underlying periodic noise. Obviously, if we measure a periodic phenomenon at instants spaced an integer multiple of its period, we will always measure the same value. By varying the observation interval, therefore, we change the sensitivity to the periodic change in the quantity measured.

In practice, if we measure a time-domain stability quantity such as the Allan variance on a timing signal affected by sinusoidal frequency modulation, the resulting plot of $\sigma_y^2(\tau)$ will exhibit a *ripple* of period T_m. Measurement results often show such ripples superposed to power-law straight slopes.

Experimental Results

A first experimental example of periodic noise is provided in Figures 5.32 and 5.33, showing results measured on the SEC of a SDH Line Terminal Multiplexer STM-16 (LTM-16). Here and in the following of the book, we will denote the supplier of this equipment as supplier A.

The measurement procedure and set-up are fully detailed in Appendix 7A. In short, a digital time counter measured the TE between the output timing signal of the Clock Under Test (CUT) and its input reference (synchronized-clock configuration). A sequence of $N = 79\,000$ samples of TE was acquired, with sampling period $\tau_0 \cong 23$ ms and over a measurement interval $T = 1800$ s. Then, ADEV and MADEV were computed with the

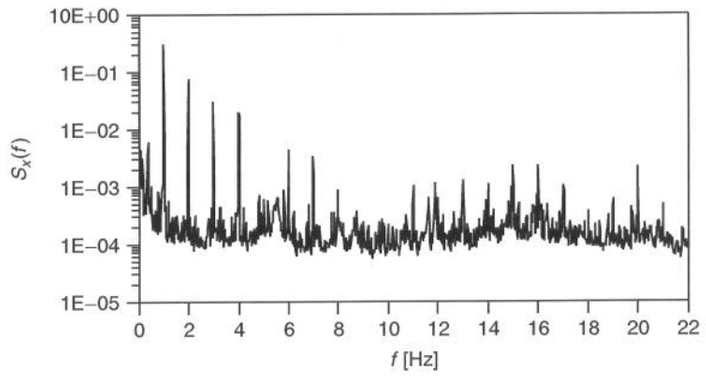

Figure 5.32. Periodic noise measured on the LTM-16 SEC from supplier A — PSD estimate $S_x(f)$ ($N = 79\,000$, $\tau_0 \cong 23$ ms, $T = 1800$ s). (Reproduced from [5.32], ©1997 IEEE, by permission of IEEE)

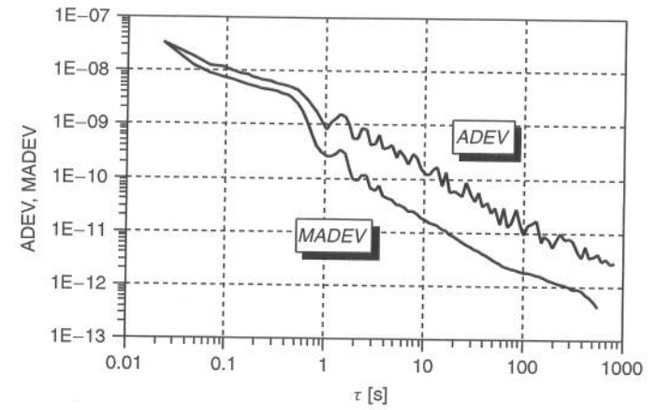

Figure 5.33. Periodic noise measured on the LTM-16 SEC from supplier A — ADEV(τ) and MADEV(τ) ($N = 79\,000$, $\tau_0 \cong 23$ ms, $T = 1800$ s). (Reproduced from [5.32], ©1997 IEEE, by permission of IEEE)

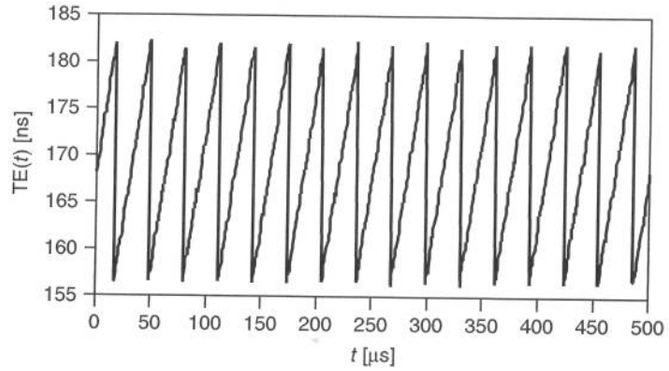

Figure 5.34. Periodic noise measured on the ADM-1 SEC from supplier B — first quarter of the TE sequence $\{x_i\}$ ($N = 4096$, $\tau_0 \cong 488$ ns, $T = 2$ ms). (Reproduced from [5.32], ©1997 IEEE, by permission of IEEE)

standard estimators of Equations (5.104) and (5.105), while the PSD $S_x(f)$ was computed (neglecting a multiplicative factor) through the Fast Fourier Transform (FFT) periodogram technique with triangular-shape data windowing.

In the frequency domain, the PSD in Figure 5.32 exhibits several discrete lines (spikes) at harmonic frequencies of about 1 Hz. In the time-domain analysis of ADEV and MADEV plots in Figure 5.33, on the other hand, the same periodic noise appears as a ripple.

A second experimental example of periodic noise is provided in Figures 5.34 through 5.36. These results were measured on the SEC of an early design of SDH Add-Drop Multiplexer STM1 (ADM1), according to the same procedure outlined above. Here and in the following of the book, we will denote the supplier of this equipment as

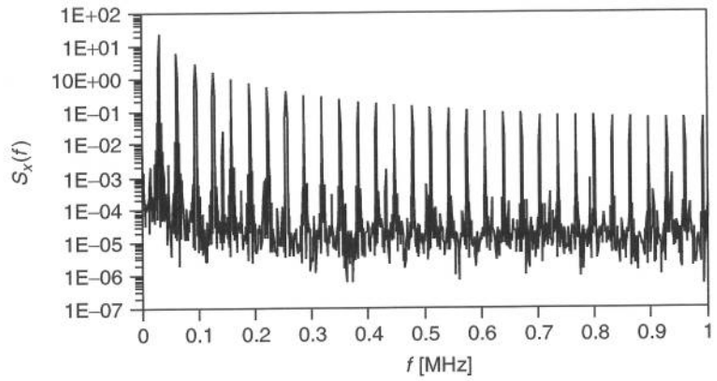

Figure 5.35. Periodic noise measured on the ADM-1 SEC from supplier B — PSD estimate $S_x(f)$ ($N = 4096$, $\tau_0 \cong 488$ ns, $T = 2$ ms). (Reproduced from [5.32], ©1997 IEEE, by permission of IEEE)

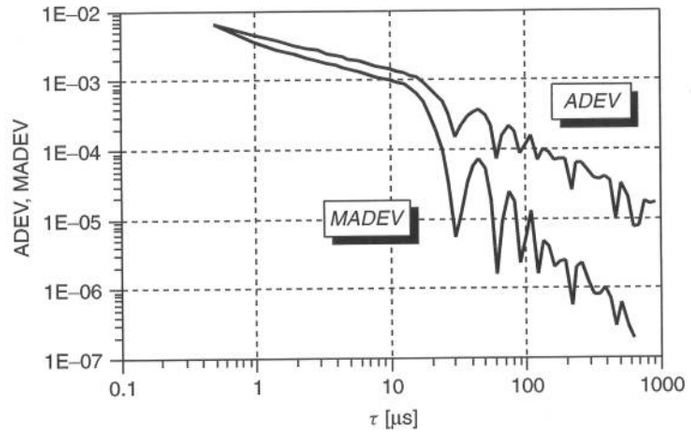

Figure 5.36. Periodic noise measured on the ADM-1 SEC from supplier B — ADEV(τ) and MADEV(τ) ($N = 4096$, $\tau_0 \cong 488$ ns, $T = 2$ ms)(Reproduced from [5.32], ©1997 IEEE, by permission of IEEE)

supplier B. This SEC was designed as DPLL, based on some numerical frequency-control algorithm producing high short-term noise. Aiming at studying the clock behaviour in the very short term, the maximum TE sampling rate was thus set, measuring the TE on *every* edge of the 2.048 MHz timing signals (thus $N = 4096$, $\tau_0 \cong 488$ ns, $T = 2$ ms).

Figure 5.34 zooms in on the first quarter (i.e., $t = 0 \div 500$ μs) of the acquired TE sequence. The plot reveals that this DPLL operates stepping alternatively between two discrete frequencies, controlled by a phase threshold mechanism. The frequency quantization error yields the saw-toothed waveform of 26-ns peak-to-peak amplitude and of period about 30–40 μs shown in the graph.

This is really a limit case, as the measured TE consists almost entirely of periodic noise. Hence, the PSD (shown in Figure 5.35) consists of a series of spikes and the ripples in the ADEV and MADEV plots (shown in Figure 5.36) are very wide. Finally, it is worthwhile noticing that such a short-term noise, when performing measurements over longer observation intervals, appears as a broadband WPM noise.

5.11 BEHAVIOUR OF THE TIME-DOMAIN STABILITY QUANTITIES: SLAVE CLOCKS

In the previous section, we described the behaviour of various time-domain stability quantities when measured on timing signals affected by power-law noise, by frequency offset and drift or by periodic noise. Such impairments model the most common non-idealities of autonomous clocks.

Now, let us suppose that the oscillator, affected for example by power-law noise, is working inside a PLL. When measurement is accomplished on the output of the slave clock, the noise generated by the internal oscillator is revealed as high-pass filtered (cf. Equation (5.75)). Thus, also the behaviour of stability quantities measured changes accordingly and is not the same anymore as reported in tables of the previous section.

Referring again to Figure 5.12, we consider three possible noise sources to investigate the behaviour of time-domain stability quantities at the output of a slave clock: the phase noise generated by the VCO ϕ_{VCO} [rad], the tension noise produced cumulatively by the phase detector and the loop filter V_{DF} [V] and the phase noise on the input signal ϕ_{in} [rad].

On the slave clock modelled in Figure 5.12, two possible measures can be envisaged. One consists of measuring the output phase noise $\phi_{\mathrm{out}}(t)$, compared to the absolute time t (in practical measurements, this can be supplied by some 'good' external reference clock). The other consists of measuring the phase error $\phi_{\mathrm{out}}(t) - \phi_{\mathrm{in}}(t)$, based on $\phi_{\mathrm{in}}(t)$ itself to establish the reference time. In ITU-T and ETSI standards [5.39][5.42], the former measurement scheme is called *independent-clock configuration*, the latter *synchronized-clock configuration*. The latter scheme, moreover, is of particular interest because it allows to observe directly the impairments added by the slave clock, without having to deal with frequency offsets between the clock under test and the reference clock.

For the sake of simplicity, we limit our analysis to the following cases, where only one noise source is considered active at a time:

(1) measurement in independent-clock configuration with only some noise $\phi_{\mathrm{VCO}}(t)$ from the VCO;

(2) measurement in independent-clock configuration with only some noise $V_{\mathrm{DF}}(t)$ from the phase detector and the loop filter;

(3) measurement in synchronized-clock configuration with only some phase noise $\phi_{\mathrm{in}}(t)$ on the reference signal

In case (1), noise from the VCO is transferred to the measured quantity ϕ_{out} *high-pass filtered* according to the transfer function $H_{\mathrm{B}}(s)$ of Equation (5.75). In case (2), noise from the phase detector and the loop filter is transferred to the measured quantity ϕ_{out}

low-pass filtered according to the transfer function $H_A(s)$ of Equation (5.74). In case (3), phase noise on the reference signal is transferred to the measured quantity $\phi_{out} - \phi_{in}$ *high-pass filtered* according to the transfer function

$$H_C(s) = \frac{\phi_{out}(s) - \phi_{in}(s)}{\phi_{in}(s)} = H(s) - 1 \tag{5.137}$$

i.e., the same as in case (1) neglecting the sign.

The behaviour of time-domain stability quantities in the three measurement schemes above can be studied as we did for autonomous clocks, by evaluating the integral relationships provided in Equation (5.113) for the true variance, in Equation (5.114) for the M-sample variance, in Equation (5.115) for the Allan variance, in Equation (5.117) for the modified Allan variance, in Equation (5.120) for the Time variance and in Equation (5.121) for the TIErms. In this case, nevertheless, the noise spectrum $S_y(f)$ in those integral relationships must be replaced by the spectrum of noise signals $\phi_{VCO}(t)$, $V_{DF}(t)$ and $\phi_{in}(t)$, properly filtered as indicated in the previous paragraph.

In conclusion, the integral relationships are evaluated by letting

$$S_y(f) = \begin{cases} S_{\phi_{VCO}}(f)|H_B(s)|^2 & \text{in case (1)} \\ S_{V_{DF}}(f)|H_A(s)|^2 & \text{in case (2)} \\ S_{\phi_{in}}(f)|H_C(s)|^2 & \text{in case (3)} \end{cases} \tag{5.138}$$

For example, we evaluated the integral relationships in the most common case of power-law noise in a second-order PLL, with closed-loop transfer function $H(s)$ characterized by bandwidth B. Examination of results allows to identify the asymptotic behaviour of the time-domain stability quantities, i.e. the corresponding power laws in the time domain as we did in the previous section for autonomous clocks.

For the sake of brevity, we report only the resulting slopes of the Allan variance and of the TIErms [5.47], in Tables 5.10 and 5.11 respectively, compared with the unfiltered slopes already reported in the previous section. Among power-law noise types, RWFM has not been evaluated for cases (1) and (3), because, on the one hand, this noise type is mostly negligible for $\tau \ll 1/B$ for all practical values of the PLL bandwidth and, on the other hand, it is filtered out as other noise types for $\tau \gg 1/B$. Moreover, in case (2), only computations for WPM and PPM were carried out, because

Table 5.10 Time-domain power laws for the Allan variance measured in slave clocks

		Cases (1) and (3)		Case (2)	
Noise Type	Unfiltered	$\tau \ll 1/B$	$\tau \gg 1/B$	$\tau \ll 1/B$	$\tau \gg 1/B$
WPM	τ^{-2}	τ^{-2}	τ^{-2}	τ^{-2}	τ^{-2}
FPM	τ^{-2}	τ^{-2}	τ^{-2}	τ^{0}	τ^{-2}
WFM	τ^{-1}	τ^{-1}	τ^{-2}	—	—
FFM	τ^{0}	τ^{0}	τ^{-2}	—	—

—= Not evaluated

Table 5.11 Time-domain power laws for the TIErms measured in slave clocks

		Cases (1) and (3)		Case (2)	
Noise Type	Unfiltered	$\tau \ll 1/B$	$\tau \gg 1/B$	$\tau \ll 1/B$	$\tau \gg 1/B$
WPM	τ^{0}	τ^{0}	τ^{0}	τ^{+1}	τ^{0}
FPM	τ^{0}	τ^{0}	τ^{0}	τ^{+2}	τ^{0**}
WFM	τ^{+1}	τ^{+1}	τ^{0}	—	—
FFM	*	τ^{+2}	τ^{0}	—	—

*Not convergent
**Depending on the loop filter
—= Not evaluated

these seem to be the only noise types encountered in practical PLL phase detectors and loop filters.

5.12 CHAINS OF SLAVE CLOCKS

In synchronization networks, chains of slave clocks are very common and are the basic architecture to transfer timing along synchronization trails (cf. the synchronization network reference chain). Hence the need to assess the performance of timing transfer along chains of slave clocks.

In this section, this complex topic is introduced and some basic result is provided. For further information, the reader may refer for example to the papers [5.48][5.49], which report studies carried out by numerical analysis and simulation under the simple hypothesis of linear behaviour of the slave clocks (i.e., the linear model of PLL is adopted). Moreover, the paper [5.50] studies random noise accumulation in chains of clocks by a time-domain state-space approach and by considering both linear and non-linear PLL models with additive noise sources.

To study the behaviour of clock chains, we present the simple models adopted by Carbonelli *et al.* in papers [5.48][5.49]. Although the assumption of linear behaviour is quite limiting, as it implies the assumption of small-amplitude phase noise, yet some indicative results can still be derived.

First, the model of clock chain is shown in Figure 5.37. A chain of K slave clocks is considered and the *synchronized-clock configuration* for relative TE measurement is adopted: the timing signal output by the Kth Slave Clock (SC) of the chain is compared to the input reference from a Reference Clock (RC). The timing signal at the input of the chain is affected by phase noise with PSD $S_{\varphi_{in}}(f)$ [rad^2/Hz]. On the other hand, the PSD of the phase noise at the output of the jth clock of the chain is denoted with $S_{\varphi out,j}(f)$ (for $j = 1, 2, \ldots, K$).

Under the assumption of clock linear behaviour, the model of the single slave clock of the chain can be derived directly from the model described in Section 5.5.5 and shown in Figure 5.12. Hence, the model for noise generation and filtering in the single slave clock is shown in Figure 5.38. In this figure, as before, φ_{in} and φ_{out} [rad] represent the phase noise on the input and output signals, φ_{VCO} [rad] is the phase noise generated by the VCO

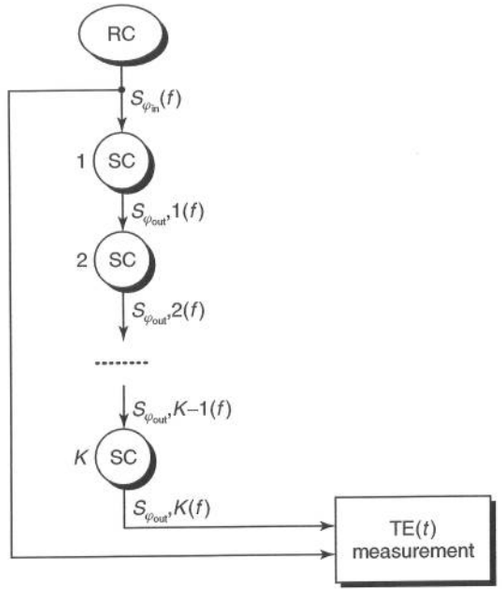

Figure 5.37. Model of chain of slave clocks with TE measurement in the synchronized-clock configuration

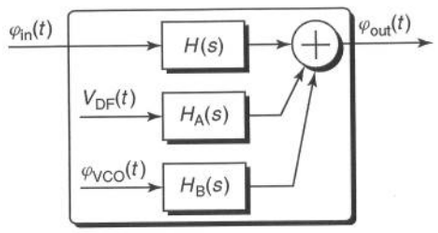

Figure 5.38. Model for noise generation and filtering in the single slave clock of the chain

and V_{DF} [V] is the tension noise produced cumulatively by the phase detector and the loop filter. Let $S_{\varphi_{in}}(f)$, $S_{\varphi_{out}}(f)$, $S_{\varphi_{VCO}}(f)$ and $S_{V_{DF}}(f)$ denote their PSDs, respectively. Finally, $H(s)$, $H_A(s)$ and $H_B(s)$ are the three transfer functions defined in Equations (5.73), (5.74) and (5.75).

Therefore, by the superposition principle, the PSD $S_{\varphi_{out}}(f)$ of the phase noise $\varphi_{out}(t)$ at the output of the clock is obtained as

$$S_{\varphi_{out}}(f) = S_{\varphi_{in}}(f)|H(f)|^2 + S_{V_{DF}}(f)|H_A(f)|^2 + S_{\varphi_{VCO}}(f)|H_B(f)|^2 \tag{5.139}$$

where transfer functions in the Fourier-frequency domain have been used, by letting $s = j2\pi f$.

Now, under the further assumption that all clocks of the chains are characterized by the same parameter values (*homogeneous chain*), it is possible to evaluate the PSD $S_{\varphi_{out},K}(f)$

of the phase noise at the output of the last clock of the chain, as

$$\begin{aligned} S_{\varphi_{out},K}(f) &= S_{\varphi_{in}}(f)|H(f)|^{2K} + \left[S_{V_{DF}}(f)|H_A(f)|^2 + S_{\varphi_{VCO}}(f)|H_B(f)|^2\right] \\ &\quad \cdot \left[\sum_{j=0}^{K-1} |H(f)|^{2j}\right] \\ &= S_{\varphi_{in}}(f)|H(f)|^{2K} + \left[S_{V_{DF}}(f)|H_A(f)|^2 + S_{\varphi_{VCO}}(f)|H_B(f)|^2\right] \\ &\quad \cdot \left[\frac{1-|H(f)|^{2K}}{1-|H(f)|^2}\right] \end{aligned} \tag{5.140}$$

Based on this expression and remembering the relationships (5.76), it is then possible to evaluate the trends of the time-domain stability quantities of interest at the output of the chain, by way of the integral relationships provided in Equation (5.113) for the true variance, in Equation (5.114) for the M-sample variance, in Equation (5.115) for the Allan variance, in Equation (5.117) for the modified Allan variance, in Equation (5.120) for the Time variance and in Equation (5.121) for the TIErms.

Nevertheless, analytical evaluation of such expressions by closed-form integration is unfeasible. Thus, paper [5.48] provides some results obtained by numerical integration, for realistic values of clock model parameters based on measurement results and manufacturer data sheets.

In particular, chains of both SEC- and SASE-type clocks were considered. Parameter values were chosen as follows: clock nominal frequency $\nu_n = 5$ MHz, PLL damping ratio $\zeta = 3$ and bandwidth $B = 1$ Hz for the SEC and $B = 1$ mHz for the SASE. Moreover, $\varphi_{VCO}(t)$ and $V_{DF}(t)$ were modelled by way of the following power-law PSDs:

$$\begin{aligned} \text{SEC}: &\begin{cases} S_{V_{DF}}(f) = \dfrac{10^{-13}}{f} + 10^{-17} \quad [\text{V}^2/\text{Hz}] \\ S_{\varphi_{VCO}}(f) = \dfrac{10^{-5.5}}{f^3} + \dfrac{10^{-12.2}}{f^2} + \dfrac{10^{-10.3}}{f} + 10^{-15.5} \quad [\text{rad}^2/Hz] \end{cases} \\ \text{SASE}: &\begin{cases} S_{V_{DF}}(f) = \dfrac{10^{-15}}{f} + 10^{-17} \quad [\text{V}^2/\text{Hz}] \\ S_{\varphi_{VCO}}(f) = \dfrac{10^{-12.2}}{f^3} + \dfrac{10^{-12.2}}{f^2} + \dfrac{10^{-13.15}}{f} + 10^{-15.5} \quad [\text{rad}^2/\text{Hz}] \end{cases} \end{aligned} \tag{5.141}$$

with upper cut-off frequency $f_h = 10$ MHz. For such values of the model parameters and with null input noise $\varphi_{in}(t) = 0$, Carbonelli *et al.* [5.48] evaluated the TIErms measured in synchronized-clock configuration (there called RTIErms according to some old terminology), according to the scheme in Figure 5.37, separately with either φ_{VCO} or V_{DF} non-null at a time.

First, a chain of M SECs was considered. The graphs in Figure 5.39(a) (φ_{VCO} internal noise only) and 5.39(b) (V_{DF} internal noise only) show the numerical results obtained for values of M from 1 to 100 and observation interval 10^{-4} s $\leq \tau \leq 10^4$ s. Notice that the stability measure results independent on the number M of clocks in the chain for $\tau \ll 1/B$, while it exhibits increasing values with M for $\tau \gg 1/B$.

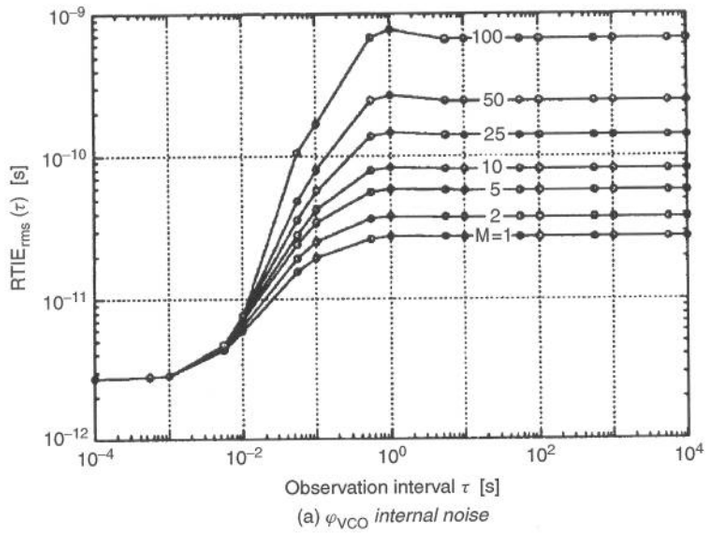

(a) φ_{VCO} *internal noise*

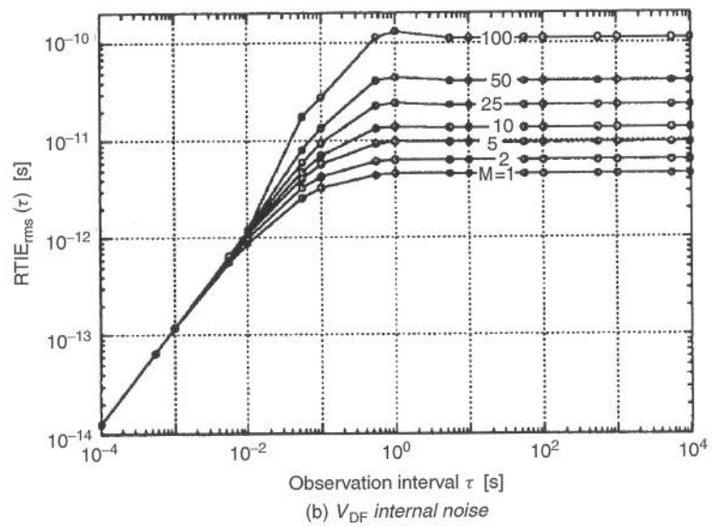

(b) V_{DF} *internal noise*

Figure 5.39. TIErms evaluated at the output of a chain of M SECs. (Reproduced from [5.48], ©1993 IEEE, by permission of IEEE)

Secondly, the effect of cascading N subchains, each made of $M = 25$ SECs and with one SASE between each subchain and the next one, was investigated. The graph in Figure 5.40 shows the results obtained for both φ_{VCO} and V_{DF} noises, for $N = 1, 2, 4$ and again for 10^{-4} s $\leq \tau \leq 10^{4}$ s. The VCO noise contribution proves to be dominant over the DF one, both in the short and in the long term, while no variations on N were found. Therefore, the heavy jitter filtering action of SASE clocks, due to their narrow bandwidth, allows to build long slave clock chains without significantly reducing the output stability.

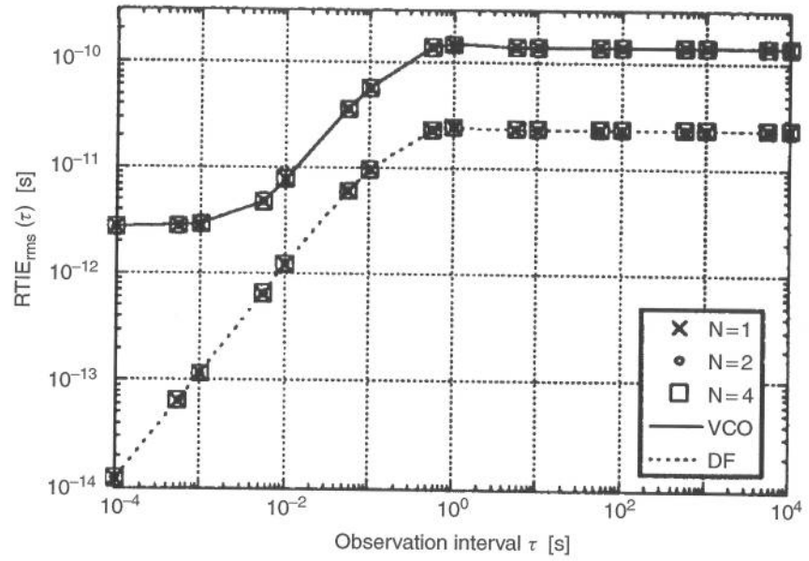

Figure 5.40. TiErms evaluated at the output of $N = 1, 2, 4$ cascaded subchains, each made of $M = 25$ SECs and with one SASE between each subchain and the next one. (Reproduced from [5.48], ©1993 IEEE, by permission of IEEE)

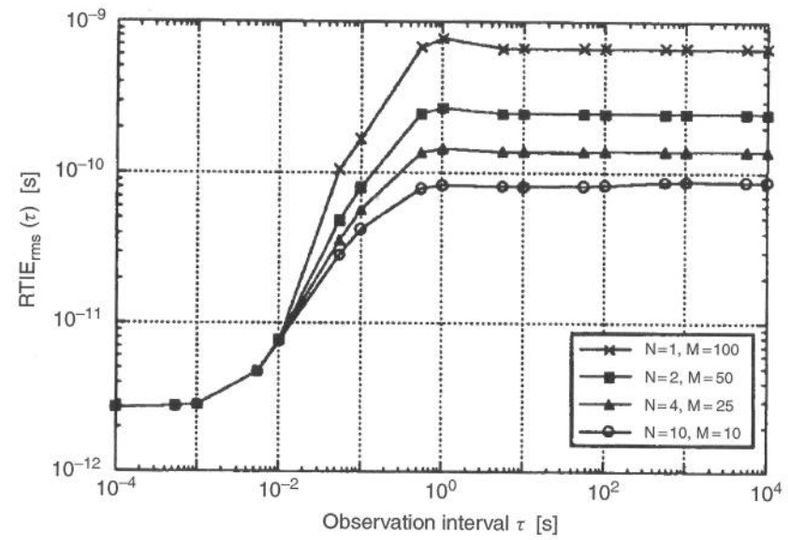

(a) φ_{VCO} *internal noise*

Figure 5.41. TIErms evaluated at the output of chains including a total of $M = 100$ SECs and $N = 1, 2, 4, 10$ SASE clocks. (Reproduced from [5.48], ©1993 IEEE, by permission of IEEE)

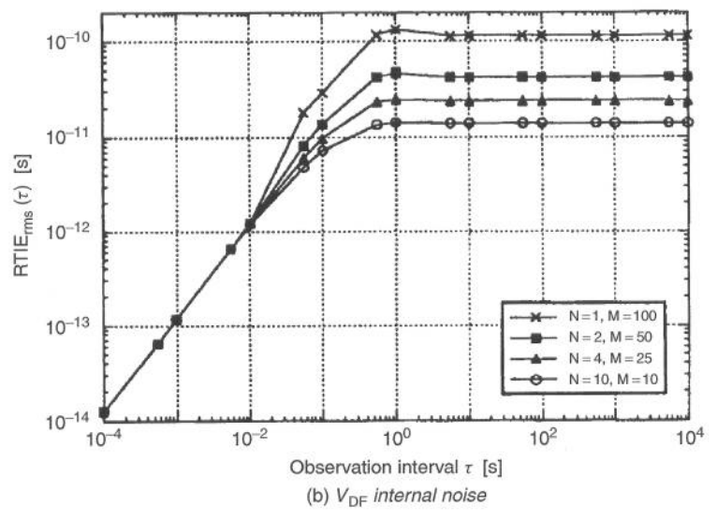

(b) V_{DF} *internal noise*

Figure 5.41. (*continued*)

Finally, referring to a worst-case chain including 100 SECs, four different combinations of subchains and SASE clocks were compared: $N = 1$ and $M = 100$, $N = 2$ and $M = 50$, $N = 4$ and $M = 25$, $N = 10$ and $M = 10$. The results are shown in Figures 5.41(a) (φ_{VCO} internal noise only) and 5.41(b) (V_{DF} internal noise only). Again, only the long-term stability results affected by the number of subchains: the bigger is the number of SECs cascaded without intervening SASE clocks, the higher is the TIErms measured. Therefore, the conclusion is that a combination with a greater number of shorter subchains should be preferred to one with fewer but longer subchains.

5.13 SUMMARY

A clock is a device able to supply a *timing signal*, i.e. a pseudo-periodic signal usable to control the timing of actions. A comprehensive model of the instantaneous frequency $\nu(t)$ supplied by actual clocks is provided in Equation (5.4).

The *stability* of a clock deals with the measurement of variations of its instantaneous frequency (or of the time generated) compared to the nominal value over a given observation interval. The *accuracy*, on the other hand, denotes the maximum frequency error $\Delta\nu_{max}$, compared to the nominal value, measured in general over the whole clock life.

An *autonomous clock* is a stand-alone device able to generate a timing signal, suitable for the measurement of time intervals, starting from some periodic physical phenomenon that runs independently of external influence. A *slave clock* is a device able to generate a timing signal, suitable for the measurement of time intervals, having phase (or much less frequently frequency) controlled by a reference timing signal at its input. The Phase-Locked Loop (PLL) and the Frequency-Locked Loop (FLL) are examples of slave clocks.

A *Phase-Locked Loop* is a control system, based on a negative feedback loop, used to automatically adjust the phase of a locally generated signal $\hat{s}(t)$ to the phase of an incoming signal $s(t)$. Its building blocks are a phase detector, a low-pass filter having

transfer function $F(s)$ and a VCO. Second-order PLLs are the most common in practi because they are able to track a constant frequency offset between the input signal and t local oscillator without residual steady-state phase error. Moreover, safe system stabil can be easily ensured. The closed-loop transfer functions $H(s) = \phi_{out}/\phi_{in}$ and $H_A(s)$ ϕ_{out}/V_{DF} are low pass, that is the input phase noise and the internal tension noise produc by the phase detector and the loop filter are low-pass filtered to the output. Converse the transfer function $H_B(s) = \phi_{out}/\phi_{VCO}$ is high pass, that is the internal phase noi generated by the VCO is high-pass filtered to the output.

A slave clock may operate in the following three modes in a synchronization netwo

- *locked mode*, when it is tracking the input frequency;
- *free-run mode*, when it has to work autonomously because the reference sign failed and the internal VCO is working with null control tension;
- *hold-over mode*, again when it has to work autonomously because the referen signal failed, but the last control tension value at the input of the VCO before t reference failure is maintained, so to hold the last output frequency value over.

The characterization of clock stability is usually carried out by characterizing, means of suitable analytical tools, the random processes $\varphi(t)$, $x(t)$, TE(t), $y(t)$ or $\nu(t$ Examples of stability measures in the *frequency domain* are the one-sided power spectr densities of the phase, time and frequency fluctuations, since they are functions of t Fourier frequency f. On the other hand, variances of the same fluctuations, averaged ov a given observation interval, are examples of stability measures in the *time domain*, sin they are functions of the observation interval τ (time).

Among the several quantities defined in the literature for characterizing time a frequency stability, the following five in the time domain have been considered b ITU-T and ETSI standard bodies: the Allan variance (AVAR), the modified Allan var ance (MAVAR), the Time variance (TVAR), the root mean square of Time Interval Err (TIErms) and the Maximum Time Interval Error (MTIE). Moreover, five standard est mators have been defined for their practical evaluation.

In the frequency domain, the model most frequently used to represent the output phas noise measured on clocks is the so-called *power-law model* (5.125). The five noise type of this model are: White Phase Modulation (WPM), Flicker Phase Modulation (FPM White Frequency Modulation (WFM), Flicker Frequency Modulation (FFM) and Randor Walk Frequency Modulation (RWFM).

The time-domain stability quantities reveal, with their characteristic trends, the presenc of the different types of power-law noise, of frequency offset and drift and of periodi noise on the signal under measurement.

5.14 REFERENCES

[5.1] J. A. Barnes, A. R. Chi, L. S. Cutler, D. J. Healey, D. B. Leeson, T. E. McGunigal, J. A Mullen Jr., W. L. Smith, R. L. Sydnor, R. F. C. Vessot, G. M. R Winkler. Characteriza tion of frequency stability. *IEEE Transactions on Instrumentation and Measurement* 197 **IM-20**(2).

[5.2] J. Rutman, F. L. Walls. Characterization of frequency stability in precision frequenc sources. *Proceedings of the IEEE*, vol. 79, no. 6, June 1991.

[5.3] D. W. Allan. Statistics of atomic frequency standards. *Proceedings of the IEEE*, vol. 54, no. 2, July 1966.
[5.4] F. L. Walls, D. W. Allan. Measurement of frequency stability. *Proceedings of the IEEE*, vol. 74, no. 1, Jan. 1986.
[5.5] J. A. Barnes. The measurement of linear frequency drift in oscillators. *Proceedings of the 15th Annual Precise Time and Time Interval (PTTI) Meeting*, 1983.
[5.6] R. L. Filler, J. R. Vig. Long term aging of oscillators. *IEEE Transactions on Ultrasonics and Ferroelectronics Frequency Control* 1993; **40**(4) 387–393.
[5.7] IEEE Std. 1139. *IEEE Standard Definitions of Physical Quantities for Fundamental Frequency and Time Metrology*. Revised version approved Oct. 20, 1988.
[5.8] International Organisation for Standardisation (ISO). *International Vocabulary of Basic and General Term in Metrology*. Geneva, 1993.
[5.9] D. W. Allan, N. Ashby, C. C. Hodge. *The Science of Timekeeping*. Application Note 1289, Hewlett-Packard Company, June 1997.
[5.10] A. J. Viterbi. *Principles of Coherent Communications*. New York: McGraw–Hill, 1966.
[5.11] W. C. Lindsey. *Synchronization Systems in Communications and Control*. Englewood Cliffs, NJ: Prentice Hall Inc., 1972.
[5.12] A. Blanchard. *Phase-Locked Loops*. New York: John Wiley & Sons, 1976.
[5.13] F. M. Gardner. *Phaselock Techniques*. New York: John Wiley & Sons, 1979.
[5.14] R. E. Best. *Phase Locked Loops*. New York: McGraw–Hill Book Company, 1984.
[5.15] P. Horowitz and W. Hill. The art of electronics, Sections 9.28 to 9.33. *Phase-Locked Loops*. Cambridge: Cambridge University Press, 1980.
[5.16] H. Meyr, G. Ascheid. *Synchronization in Digital Communications. Vol. 1: Phase-, Frequency-Locked Loops, and Amplitude Control*. New York: John Wiley & Sons, 1990.
[5.17] V. F. Kroupa. Noise properties of PLL systems. *IEEE Transactions on Communications* 1982; **COM-30**(10): 2244–2252.
[5.18] L. S. Cutler, C. L. Searle. Some aspects of the theory and measurement of frequency fluctuations in frequency standards. *Proceedings of the IEEE*, vol. 54, no. 2, Feb. 1966.
[5.19] J. A. Barnes. Atomic timekeeping and the statistics of precision signal generators. *Proceedings of the IEEE*, vol. 54, no. 2, Feb. 1966.
[5.20] P. Lesage, C. Audoin. Characterization of frequency stability: uncertainty due to the finite number of measurements. *IEEE Transactions on Instrumentation and Measurement* 1973; **IM-22**(2).
[5.21] W. C. Lindsey, C. M. Chie. Theory of oscillator instability based upon structure functions. *Proceedings of the IEEE*, vol. 64, no. 12, Dec. 1976.
[5.22] J. Rutman. Characterization of phase and frequency instabilities in precision frequency sources: fifteen years of progress. *Proceedings of the IEEE*, vol. 66, no. 9, Sept. 1978.
[5.23] P. Lesage, C. Audoin. Characterization and measurement of time and frequency stability. *Radio Science (American Geophysical Union)*, 1979; **14**(4): 521–539.
[5.24] D. W. Allan, J. A. Barnes. A modified Allan variance with increased oscillator characterization ability. *Proceedings of the 35th Annual Frequency Control Symposium*, 1981.
[5.25] D. A. Howe, D. W. Allan, J. A. Barnes. Properties of signal sources and measurement methods. *Proceedings of the 35th Annual Frequency Control Symposium*, 1981.
[5.26] P. Lesage, T. Ayi. Characterization of frequency stability: analysis of the modified Allan variance and properties of its estimate. *IEEE Transactions on Instrumentation and Measurement* 1984; **IM-33**(4).
[5.27] S. R. Stein. Frequency and time—their measurement and characterization. In *Precision Frequency Control*. Vol. 2, ch. 2, pp. 191–232. New York: Academic Press, 1985.
[5.28] L. G. Bernier. Theoretical analysis of the modified Allan variance. *Proceedings of the 41st Annual Symposium on Frequency Control*, 1987.
[5.29] D. B. Sullivan, D. W. Allan, D. A. Howe, F. L. Walls (eds). *Characterization of Clocks and Oscillators*. NIST Technical Note 1337, March 1990.

[5.30] D. W. Allan, M. A. Weiss, J. L. Jespersen. A frequency-domain view of time-domain characterization of clocks and time and frequency distribution systems. *Proceedings of the 45th Annual Symposium on Frequency Control*, 1991.
[5.31] M. Carbonelli, D. De Seta, D. Perucchini. Characterization of timing signals and clocks. *European Transactions on Telecommunications* 1996; **7**(1).
[5.32] S. Bregni. Clock stability characterization and measurement in telecommunications. *IEEE Transactions on Instrumentation and Measurement* 1997; **46**(6).
[5.33] S. Bregni. Measurement of maximum time interval error for telecommunications clock stability characterization. *IEEE Transactions on Instrumentation and Measurement* 1996; **IM-45**(5).
[5.34] S. M. Kay, S. L. Marple. Spectrum analysis—a modern perspective. *Proceedings of the IEEE*, vol. 69, no. 11, Nov. 1981.
[5.35] W. H. Press, B. P. Flannery, S. A. Teukolsky, W. T. Vettering. *Numerical Recipes in C—The Art of Scientific Computing*. Cambridge: Cambridge University Press. (Also available for other programming languages)
[5.36] A. Papoulis. *Probability, Random Variables and Stochastic Processes*. 2nd edition. New York: McGraw-Hill, 1984.
[5.37] ITU-T Recs. G.810 *Considerations on Timing and Synchronization Issues*; G.811 *Timing Requirements at the Outputs of Primary Reference Clocks Suitable for Plesiochronous Operation of International Digital Links*; G.812 *Timing Requirements at the Outputs of Slave Clocks Suitable for Plesiochronous Operation of International Digital Links*. Geneva, Blue Book, 1988.
[5.38] ANSI T1.101 *Telecommunications—Synchronization Interface Standard*. January 1997.
[5.39] ITU-T Rec. G.810 *Definitions and Terminology for Synchronisation Networks*. Geneva, August 1996.
[5.40] S. Bregni, F. Setti. Impact of the anti-aliasing prefiltering on the measurement of MTIE. *Proceedings of IEEE GLOBECOM '97*, Phoenix, AZ, USA, 3–8 November 1997.
[5.41] S. Bregni, S. Maccabruni. Fast computation of maximum time interval error by binary decomposition. *IEEE Transactions on Instrumentation and Measurement* 2000; **40**(6).
[5.42] EN 300 462 *Transmission and Multiplexing (TM); Generic Requirements for Synchronization Networks*; Part 1-1: *Definitions and Terminology for Synchronization Networks*; Part 2-1: *Synchronization Network Architecture*; Part 3-1: *The Control of Jitter and Wander within Synchronization Networks*; Part 4-1: *Timing Characteristics of Slave Clocks Suitable for Synchronization Supply to Synchronous Digital Hierarchy (SDH) and Plesiochronous Digital Hierarchy (PDH) Equipment*; Part 5-1: *Timing Characteristics of Slave Clocks Suitable for Operation in Synchronous Digital Hierarchy (SDH) Equipment*; Part 6-1: *Timing Characteristics of Primary Reference Clocks*.
[5.43] R. A. Baugh. Frequency modulation analysis with the hadamard variance. *Proceedings of the 25th Annual Symposium on Frequency Control*, April 1971, pp. 222–225.
[5.44] F. L. Walls, A. De Marchi. RF spectrum of a signal after frequency multiplication: measurement and comparison with a simple calculation. *IEEE Transactions on Instrumentation and Measurement* 1975; **24**(3).
[5.45] D. E. Knuth. *The Art of Computer Programming*. Vol. 2, p. 118. London: Addison-Wesley, 1981.
[5.46] J. A. Barnes, D. W. Allan. A statistical model of flicker noise. *Proceedings of the IEEE*, vol. 54, no. 2, pp. 176–178, Feb. 1966.
[5.47] S. Bregni, M. Carbonelli, D. De Seta, D. Perucchini. Impact of slave clock internal noise on Allan variance and root mean square time interval error measurement. *Proceedings of IEEE Instrumentation and Measurement Technology Conference*, Hamamatsu, Japan, 10–12 May 1994.